Three-dimensional laser creation of near-IR laser-gain medium based on hydride donor/acceptor complexes made of coupled laser-induced silver nanoclusters with Ytterbium ions

*Fouad Alassani,[1] Guillaume Raffy,[2] Mathis Carpentier,[1] Joëlle Harb,[1] Véronique Jubera,[1] André Del Guerzo,[2] Lionel Canioni,[1] Thierry Cardinal,[1] Yannick Petit[1,]**

[1] *Université de Bordeaux, CNRS, Bordeaux INP, ICMCB, UMR 5026, F-33600, Pessac, France.*
[2] *Université de Bordeaux, CNRS, Institute of Molecular Sciences (ISM, UMR 5255), F-33400, Talence, France.*

Keywords: fluorescent silver nanocluster, glass, periodic structure, direct laser writing, energy transfer, sub-diffraction limit, rare earth co-doping, hybrid systems, laser active media

Corresponding author : yannick.petit@u-bordeaux.fr

Supporting information

(A) Spatial transverse profiles of laser-induced double-track fluorescent patterns for the UV excited silver nanoclusters (visible range) and for the indirectly excited Yb^{3+} ions by energy transfer from silver nanoclusters

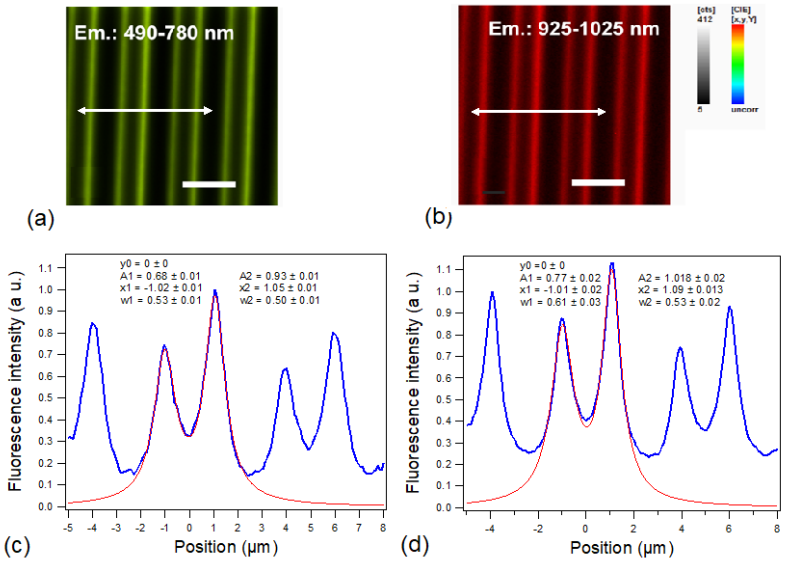

Figure S1. (a, b) Hyperspectral fluorescence image excited at 473 nm and collected for the visible silver nanocluster emission range, and in the near-IR for the near-IR Yb^{3+} emission, respectively. Scale bar : 5 µm. (c, d) 1D cross-sections of a double-track pattern for the visible range and the near-IR range, respectively, realized along the white double-arrow lines of Figs. 1(a,b).

The modeling of a fluorescent double-track profile has been set with a double Lorenztian profile, such as f(x) = y0 + A1/(1+ ((x-x1)/w1)^2) + A2/(1+ ((x-x2)/w2)^2). The obtained fitted half-width at half maxima indicate 0.5 µm typically so that the full width half maximum stands in the µm scale, both for the VIS and near-IR range.

(B) Resilience of the spatial homogeneity of the Yb^{3+} distribution fluorescence after fs laser inscription

The spatial distribution of Yb^{3+} ions has been investigated under direct excitation at 976 nm. Hyperspectral confocal microscopy has been performed along a cross-section perpendicularly to a double-track fluorescent structure, as located along the red line of **Suppl. Mater. Figure 2.**(a). Excitation was performed at 976 nm, using a 50x NA 0.9 Olympus objective with a LabRAM micro-spectrometer. Fluorescence spectra were recorded in epi-collection over the spectral range of 1000-1100 nm, for each position separated by 0.1 µm within a range of ±3.5 µm around the central part of a femtosecond laser pass. Successive femtosecond laser passes were separated by 10 µm during the inscription process, so that the tested Yb^{3+} distribution cannot be affected by surrounding laser passes.

All the recorded spectra showed exactly the same profile, without any modification in the center of the laser pass, excluding thus any environmental change of the glass matrix. Moreover, the spectra were numerically integrated : the resulting integrated fluorescence intensity in plotted in of **Suppl. Mater. Figure 2.**(b), showing minor intensity variations below 0.2%. These intensity variations showed no spatial correlations with the central position of the laser pass where one might have expected Yb^{3+} depletion, so that any potential laser-induced modification of Yb^{3+} concentration is much below the 0.2% level. The observed intensity variations are thus within the accuracy of the experiment, including the potential influence of the local laser-induced Δn that can affect the efficiency of fluorescence collection.

As a conclusion, one can say that Yb^{3+} migration due to fs laser inscription process can be neglected.

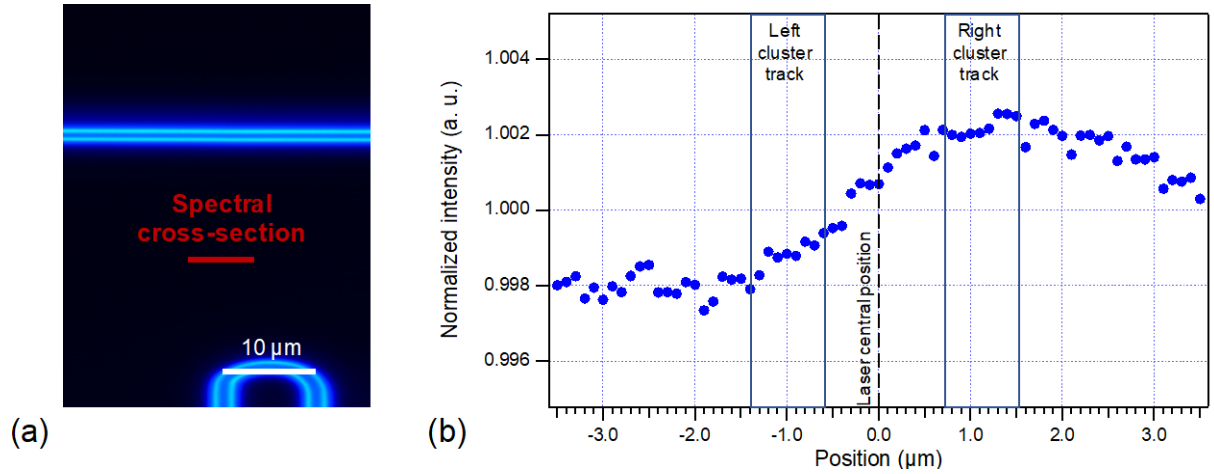

Figure S2. (a) Wide field fluorescence image of series of double-track lines inscribed by femtosecond laser, with UV excitation and visible range collection showing the localization of molecular silver nanoclusters. (b) Fluorescence intensity distribution along the 1D cross-section (red line of Fig. (a)), corresponding to an excitation at 976 nm and a collection for a spectral integration from 1000 nm to 1100 nm, and showing an absence of signature of Yb^{3+} migration under fs laser irradiation within the experimental resolution.

(C) Time-resolved fluorescence decays of silver nanoclusters and influence of the co-insertion of Yb^{3+} ions, demonstrating lifetime shortening and energy transfers from the nanoclusters to the rare earth ions.

The time-resolved fluorescence decays are shown for the 5 inter-distances of laser inscriptions both each of the two photosensitive glasses PZnAg and PZnAg:Yb. These data are extracted from time-resolved fluorescence confocal microscopy images of Figs. 3(a) and 3(b).
The resulting fitting (not shown here) with the three-exponential decay model has led to the associated fitting parameters are gathered in Table 1. The three-exponential decays appeared to be the most reasonable model (compared to two- or four-exponential decays), taking into account the achieved quality of the fits. This model was systematically applied the same way to each experimental pattern of Figs. 3(a,b) so as to minimize any influence of the numerical approach.

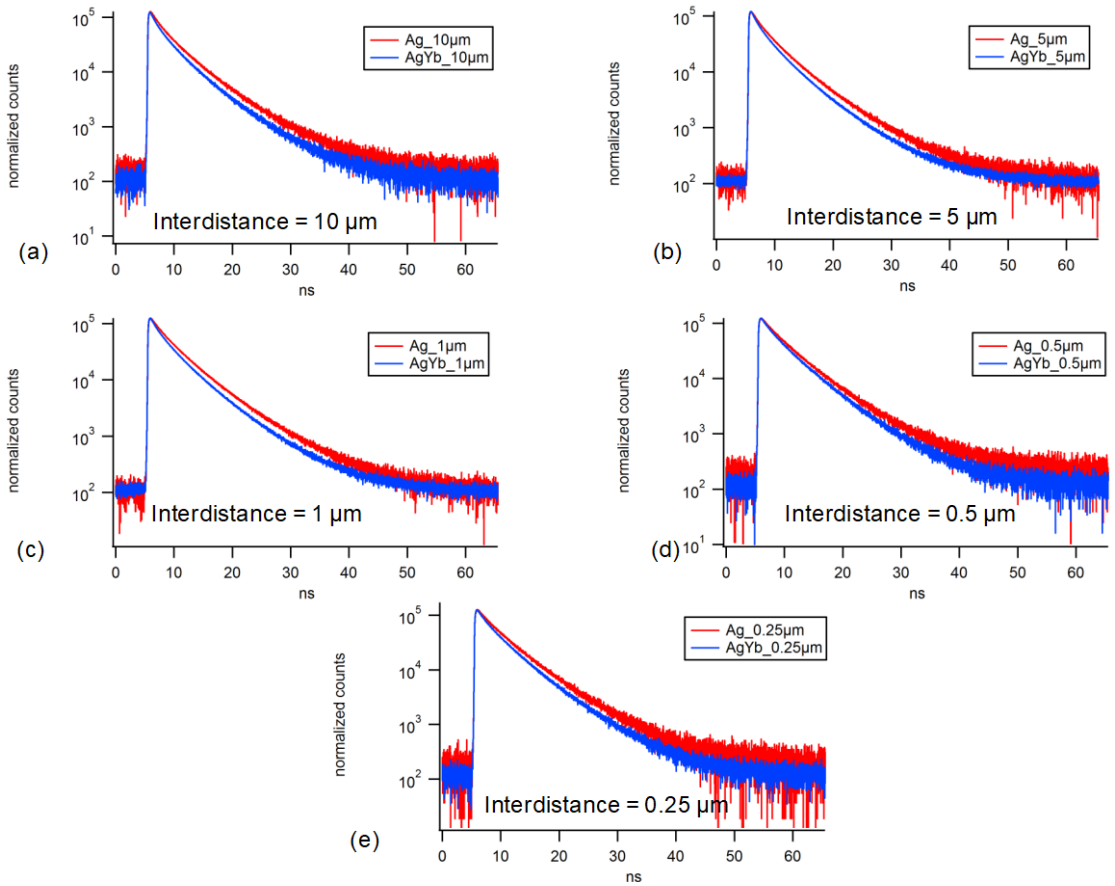

Figure S3. Fluorescence decays of laser-inscribed silver nanoclusters in both the PZnAg and PZnAg:Yb glasses. All data were obtained with a 375 nm pulse excitation of 120 ps at 5 MHz with collection over 400-600 nm. (a,b,c,d) Inter-distances between successive laser passes from 10, 5, 1, 0.5 and 0.25 nm, respectively.

(D) Visualization of the fitted parameters of Table 1, to show the overall consistency of the extracted set of parameters in the three-exponential decay model to depict the fluorescence lifetime decays of silver nanocluster patterns with and without the presence of Yb^{3+} ions.

Each of the three involved lifetimes shows a typical monotonic shortening trend while considering shorter overlapping distances during laser inscription. Each of the three involved lifetimes shows also a shortening trend while introducing the Yb3+ ions (compare **Suppl. Mater. Figs. 4(a)** and **4(b)**). The relative weight of each fluorescence lifetime are relatively stable over the set of experimental conditions, and reasonably comparable with/without Yb^{3+} ions.

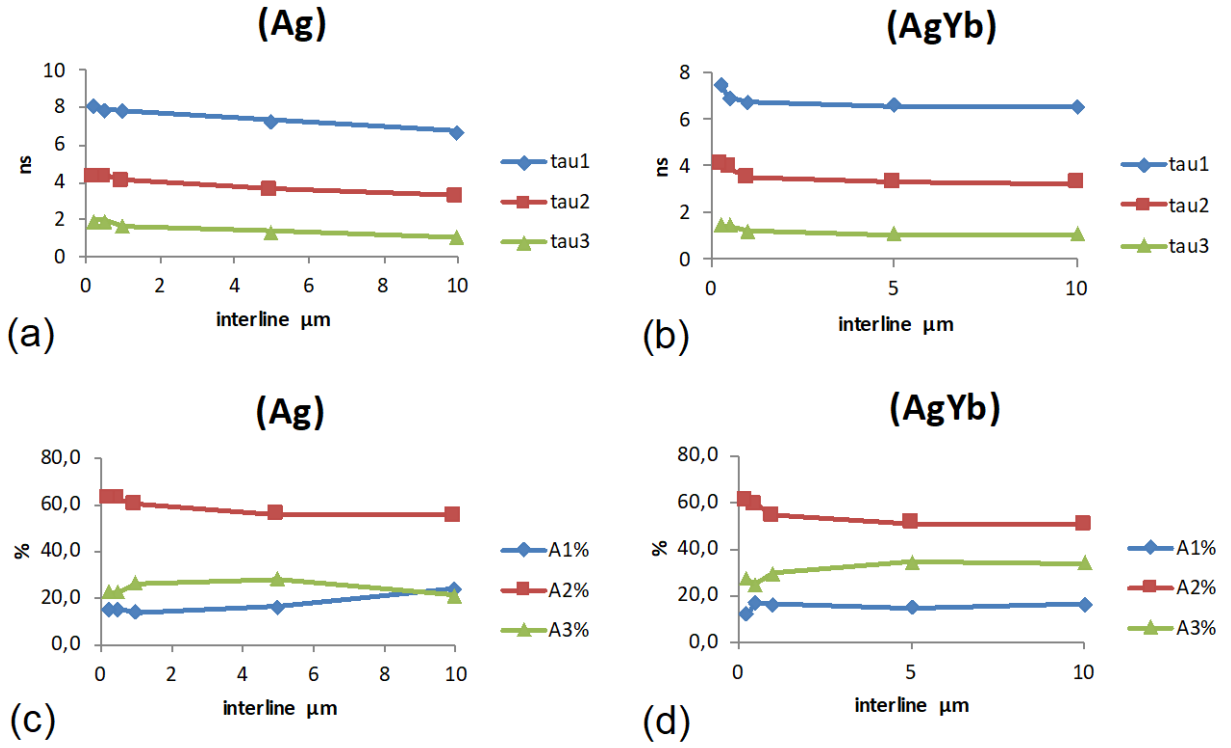

Figure S4. Extracted parameters (both amplitudes and fluorescence lifetimes) with the three-exponential decay model to fit the fluorescence decays of laser-inscribed silver nanoclusters in both the PZnAg and PZnAg:Yb glasses. All data were obtained with a 375 nm pulse excitation of 120 ps at 5 MHz with collection over 400-600 nm. (a,b,c,d) Inter-distances between successive laser passes from 10, 5, 1, 0.5 and 0.25 nm, respectively.

(E) Effective gain cross section depending on the population inversion rate of the lasing transition of the Yb^{3+} ions.

Absorption spectrum was directly measured with standard macroscopic transmission with the pristine Yb^{3+}-doped silver-containing phosphate glass. Absorption cross-section was obtained with the absorption spectrum and the Yb^{3+} concentrations (inversion population rate $\beta = 0$). The emission cross-section was estimated taking into account standard reciprocity and Füchtbauer-Ladenburg methods (inversion population rate $\beta = 1$). Such inversion population rate can be set to any value between 0 and 1.

In the case of three-level systems such as Yb^{3+} ions, the effective cross-section is depicted as $\sigma_{eff.}(\beta;\lambda) = \beta.\sigma_{em.}(\lambda) - (1-\beta)\sigma_{abs.}(\lambda)$. The optically-induced transparency is achieved for an inversion population $\beta_{transp.} = \frac{\sigma_{abs.}}{\sigma_{abs.}+\sigma_{em.}}$ for which $\sigma_{eff.}(\beta_{transp.};\lambda) \equiv 0$.

With the involved absorption and emission cross-sections ($\sigma_{abs.}$ = 0.0434×10^{-20} cm^2 and $\sigma_{em.}$ = 0.454×10^{-20} cm^2, respectively) at the standard Yb^{3+} lasing wavelength (namely at 1030 nm), the optically-induced transparency, for which the effective cross-section becomes null, is expected to be achieved of an inversion population rate $\beta_{transp.}^{1030nm}$ = 8.5%.

Note that the relative gain coefficient in a non-saturated "small signal" gain condition writes $\Delta g_0 = g(\beta) - g(\beta = 0) = N_0^{Yb^{3+}}\left(\sigma_{eff.}(\beta) - \sigma_{eff.}(\beta = \mathbf{0})\right) = N_0^{Yb^{3+}}\beta(\sigma_{em.} + \sigma_{abs.})$.

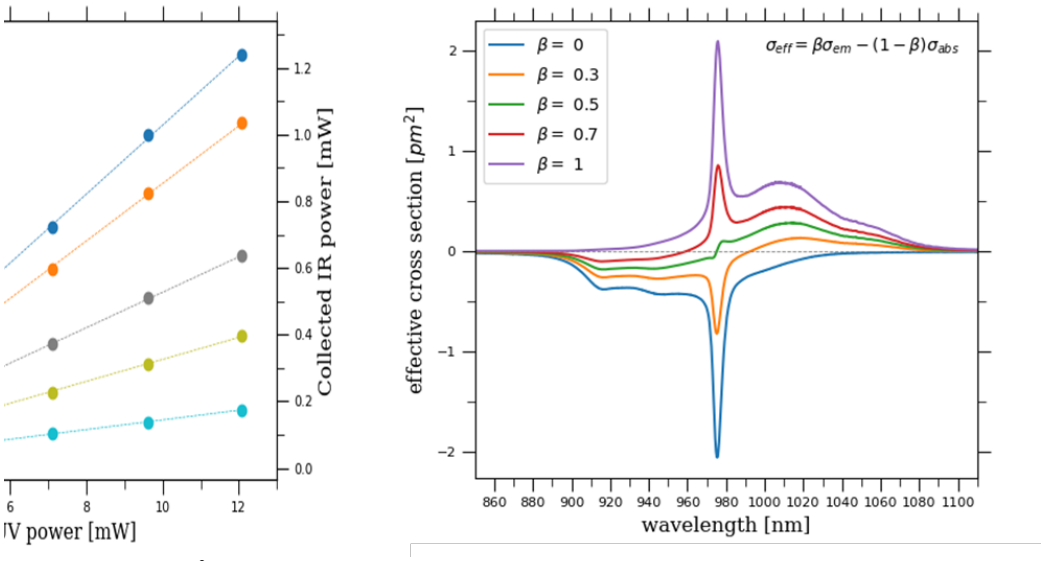

Figure S5. Effective gain cross section of Yb^{3+} ions in the PZnAg:Yb glass, showing absorption (negative values) and emission (positive values) cross sections for an inversion rate of 0 (blue), 0.3 (orange), 0.5 (green), 0.7 (red) and 1 (purple), respectively.

(F) Estimation of the linear absorption coefficient of the adapted waveguides, for a UV pumping radiation at 405 nm.

In the case of single-pass laser inscription, the linear absorption coefficient typically stands in the 300-600 cm^{-1} within each laser pass at the UV pumping wavelength (namely at 405 nm)[31,35]. Because the considered waveguide has been produced with a 3 µm lateral width with successive overlapping laser passes separated by 250 nm each (see Experimental Section), one has to consider results from Fig. 2(d)) where silver nanocluster fluorescence is shown to drop severely when laser overwriting occurs. With a laser pass inter-distance of 250 nm, fluorescence emission is only 3.2 % compared to single-pass patterns. By assuming that such a fluorescence emission drop results only by the drop of absorption due to an effectively lower silver nanocluster concentration, one can rescale the expected absorption taking place in the waveguide. Therefore, the local linear absorption coefficient α^{UV} at 405 nm in the considered waveguide is estimated to 10-20 cm^{-1}, typically corresponding to an effective length $L_{eff}^{UV} = 1/\alpha^{UV}$ of 0.05-0.1 cm, with α^{UV} the linear absorption coefficient of the waveguide at the UV pumping wavelength (namely at 405 nm).